
Article:
Jenkinson, D.R., Cadby, A. and Jones, S. (2017) The synthesis and photophysical analysis of a series of 4-nitrobenzochalcogenadiazoles for super-resolution microscopy. Chemistry - A European Journal . ISSN 0947-6539

https://doi.org/10.1002/chem.201702289

CHEMISTRY
A European Journal

A Journal of
ChemPubSoc Europe

Accepted Article

Title: The synthesis and photophysical analysis of a series of 4-nitrobenzochalcogenadiazoles for super-resolution microscopy

Authors: Daniel Ray Jenkinson, Ashley Cadby, and Simon Jones

To be cited as: *Chem. Eur. J.* 10.1002/chem.201702289

Link to VoR: http://dx.doi.org/10.1002/chem.201702289

Supported by
ACES

WILEY-VCH

10.1002/chem.201702289

WILEY-VCH

The synthesis and photophysical analysis of a series of 4-nitrobenzochalcogenadiazoles for super-resolution microscopy

D. R. Jenkinson,[a] A. J. Cadby,*[b] and S. Jones*[a]

Abstract: A series of 4-nitrobenzodiazoles with atomic substitution through the chalcogen group were synthesised and their photophysical properties analysed with a view for use in single-molecule localisation microscopy. Sub-diffraction resolution imaging was achieved for silica nanoparticles coated with each dye. Those containing larger atoms were favoured for super-resolution microscopy due to a reduced blink rate (required for stochastic events to be localised). The sulfur containing molecule was deemed most amenable for widespread use due to the ease of synthetic manipulation compared to the selenium containing derivative.

Introduction

Fluorescence microscopy is commonly used in biology for non-invasive imaging as the biochemical specificity of fluorescent probes is often easily tuned.[1–3] Fluorophores add contrast to images and have been used to visualise biological systems at a microscopic level, however optical resolution is limited by diffraction.[4] The development of single-molecule localisation microscopy (SMLM) techniques such as STORM,[5] PALM,[6] and FPALM[7] has enabled the analysis of biological structures and processes with lateral resolutions on the nanometre scale. These techniques exploit triggered emission switching (photoblinking), an effect thought to arise as the result of a stable dark state. This allows only a small subset of fluorophores to exist in an emissive "on-state," and each can be localised to reconstruct a high-resolution image.[5] For example, two dark states have been identified for cyanine 5 (Cy 5), of which one is a triplet state accessed *via* inter-system crossing and is accessed considerably quicker in the presence of iodide due to heavy-atom-induced spin-orbit coupling.[8] The other was recognised as a *trans-cis* isomerisation to a non-fluorescent isomer. Cy 5 can be reversibly switched between its on- and off-states with a high degree of control.[9] The induced dark state has a lifetime in the order of hours in the absence of oxygen that suggested the existence of another energy level accessed *via* the triplet state since this lifetime is much longer than other reported triplet states compared in this work (on the order of 100 milliseconds). A similar observation was also made in a separate study using rhodamine dyes.[10] Given the importance of this technique in modern biology, it has become imperative to investigate the structure-function relationship for the photoblinking activity of dyes.

Atomic substitution down the chalcogen group has previously been used as a method of tailoring the fluorescence properties of oxygen containing dyes to induce a bathochromic shift in the absorption and emission spectra.[11–14] Though red-shifting is achieved, quantum yield and extinction coefficient are vastly reduced owing to more stable triplet states.[15] Such atomic substitution also leads to atoms with larger and more diffuse orbitals, which has interesting effects on the aromatic nature of these species.[16] Substitution of oxygen for sulfur and selenium in 2,1,3-chalcogenodiazoles has been shown theoretically and experimentally to increase the degree of aromaticity in the heteroaromatic systems.[17–19] Sulfur containing compounds appear to be almost twice as aromatic using Bird's unified aromaticity index (I_A) than the oxygen containing analogues due to a vastly decreased electronegativity. This effect is, however, negated in 2,1,3-selenadiazole since its much larger atomic size and more diffuse orbitals diminish the ability to delocalize electrons, meaning that the selenium containing compound has a much lower aromaticity than the sulfur containing compound, but is still slightly higher than the oxygenated derivative (I_A = 53, 104, and 58 for X = O, S, and Se, respectively).[19] By making valence isoelectronic substitutions down a period it was hoped to have an influence on the strength of the aromaticity, which could be measured by observing differences in key photophysical properties. Thus, in order to investigate atomic substitution was the sole cause of any photophysical difference, 4-nitrobenoxadiazole (NBD) frameworks were investigated where the planar structure should negate any flexibility in the molecule that may arise from torsion or twisting that may also disturb aromaticity. This moiety is commonly used as a fluorescent probe due to its small molecular mass, high cell permeability and large stokes shift but has not yet been used in super-resolution techniques.[20]

Results and Discussion

Molecular modelling was first conducted to examine the structural framework of the target systems. This confirmed the hypothesis that when oxygen is substituted for sulfur and selenium, the aromatic system remains planar but the ring in which the chalcogen is contained distorts within the plane in order to accommodate the larger atom (Table 1, see supplementary information for geometrically optimised structures).[21] On this basis, a series of 4-nitrobenzochalcogenadiazoles were targeted that included a group capable of being ligated to a nanoparticle for later visualization. This was planned to be introduced *via* S_NAr reaction of (3-aminopropyl)triethoxysilane (APTES) with the corresponding aryl-halide to give a siloxane terminus leading to compounds **1** (NBD-APTES), **2** (NPT-APTES) and **3** (NPSe-

[a] Mr. D. R. Jenkinson, Prof. S. Jones*
Department of Chemistry
University of Sheffield
Dainton Building, Brook Hill, Sheffield, S3 7HF, United Kingdom
E-mail: simon.jones@sheffield.ac.uk
[b] Dr. A. J. Cadby*
Department of Physics and Astronomy
University of Sheffield
Hicks Building, Hounsfield Rd., Sheffield, S3 7RH, United Kingdom
E-mail: a.cadby@sheffield.ac.uk

Supporting information for this article is given via a link at the end of the document.

APTES) in preparation for ligation to silica nanoparticles which are optically inert and easy to functionalise.

Table 1. Results of energy calculations and geometry optimisation. [a]

X	LUMO–HOMO difference (eV)	λ_{max} (nm)	N-X-N bond angle (°)	N-X bond length (Å) [b]
O	3.2014	386	113.0	1.365
S	3.2509	380	99.4	1.638
Se	3.0403	406	93.5	1.801

[a] Calculated using Gaussian 09.[22] [b] Taken as an average of the two N-X bonds.

NBD-APTES **1** was prepared in one step from the commercially available 4-chloro-7-nitrobenzo-2,1,3-oxadiazole (NBD-Cl) and APTES as previously reported in the literature (Scheme 1).[23]

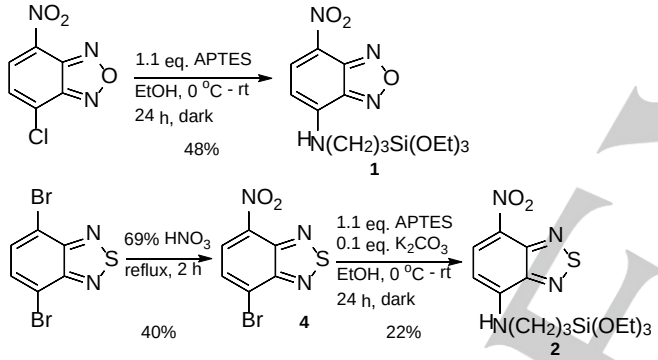

Scheme 1. Synthesis of dyes **1** and **2**.

NPT-APTES **2** was synthesised in two steps from 4,7-dibromobenzo-2,1,3-thiadiazole and required the addition of a base to improve the yield of the S_NAr reaction (Scheme 1). However, the selenium containing target **3** was more challenging since the 1,4-nitrohalide **6** was not commercially available. This was accessed by adapting a reported procedure *via* vicarious nucleophilic substitution and selenium insertion (Scheme 2).[24] However, a series of S_NAr conditions failed to produce the desired target. NPSe-APTES **3** was instead accessed *via* a palladium catalysed aromatic amination,[25] which was successful for the halo derivatives of all three heteroaromatic systems when using THF as the solvent. Although the yield of this reaction was poor, sufficient material was obtained for the necessary measurements.

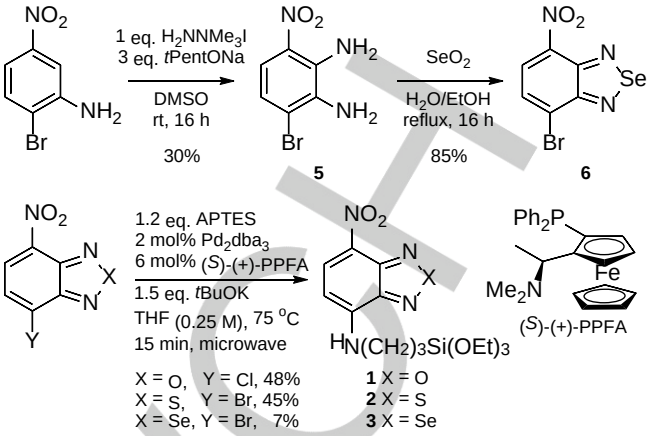

Scheme 2. Preparation of precursor **6** and aromatic amination reactions to prepare targets **1**-**3**.

The chemical shifts of the aromatic protons for each of the three compounds support an increased degree of aromaticity for those with heavier atoms.[26] Peaks attributed to the aromatic protons were shifted most downfield in compound **2**, with the protons in compound **1** being the most upfield, suggesting a lower degree of deshielding and hence a lower degree of aromaticity (δ_{ArH} = 8.48 and 6.17, 8.67 and 6.41, 8.62 and 6.17 for **1**, **2** and **3** respectively). The solution phase absorption and emission spectra for NBD-APTES **1** and NPT-APTES **2** were found to be comparable, but NPSe-APTES **3** was highly red-shifted (Figure 1). This effect has been observed with selenium analogues of D-luciferin and attributed to the polar effect.[12,27] It is noted that, although the measured absorption maxima are not exactly in line with the predicted values, the energy calculations did predict that the maxima for **1** and **2** would be close to each other, and that λ_{max} for compound **3** would be red shifted. Compound **2** absorbing at a lower wavelength than compound **1** was also predicted.

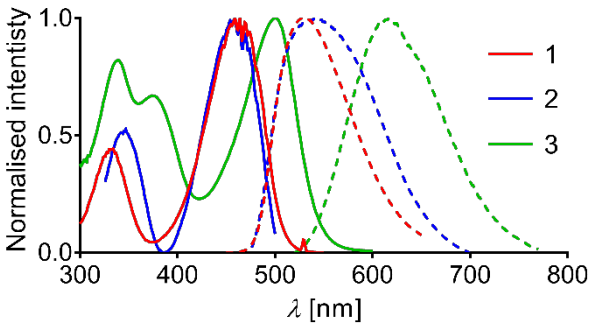

Figure 1. Normalised absorption (solid lines) and emission (dashed lines) for compounds **1**, **2**, and **3**.

A decrease in molar extinction coefficient was observed when heavier atoms were incorporated, in broad agreement with other dyes with substitution patterns down the chalcogen group.[11–14] (Table 2). The molecules containing heavier atoms have vastly decreased extinction coefficients. According to Nijegorodov and Mabbs, the introduction of a heavier atom may decrease the oscillator strength for the $S_0 \rightarrow S_1$ transition due to changes in the parameters of matrix elements in the molecular orbital, therefore making absorption less likely.[28,29]

Table 2. Measured photophysical properties of compounds **1**, **2**, and **3**.

Dye	λ_{max} [a] Abs	Em	ε (M^{-1} cm^{-1}) [b]	Φ (%) [c]	τ (ns)
1	465	542	24,000	0.8	2.6
2	460	550	1,400	0.2	1.1
3	500	615	3,900	0.2	1.7

[a] Absorption and emission were measured using 100 µM solutions. [b] Molar extinction coefficients were extrapolated from calibration curves plotted using solutions with concentrations between 10-100 µM and are correct to two significant figures. [c] Quantum yield measurements taken using an integration sphere and compared to a highly fluorescent dye with a known quantum yield. [d] Excited state lifetime measurements were taken using a time-correlated single photon counting method for time-resolved photoluminescence.

Similarly, there was a drop in the quantum yield when larger atoms were incorporated due to a higher probability of transfer to the triplet state *via* intersystem crossing (ISC), though the method used to measure the excited state lifetime was not accurate enough to allow more precise quantities to be taken.
Though there was little variation between the three molecules it was clear that oxygen containing NBD-APTES **1** had the longest excited state lifetime, indicating that fluorescence may be favoured rather than undergoing ISC to the dark state. The rate of photobleaching was measured using a method described by Sauer *et al*.[30] in which solutions of dyes are bleached using a laser and reactivated by reincorporation of oxygen by agitation in the presence of different buffer solutions. When dissolved in distilled water there was negligible decay in fluorescence intensity of the sulfur and selenium containing dyes, even when using high laser powers. Interestingly, it was observed that NBD-APTES **1** showed an increase in fluorescence intensity to a plateau with continued laser irradiation over 40 minutes at all concentrations and laser intensities used (Figure 2). This may be the result of an intermolecular FRET like mechanism arising from the slight overlap in the absorption and emission spectra between closely associated molecules. However, since compounds **2** and **3** do not exhibit this behavior but also have overlapping absorption and emission spectra this is less probable. Similar observations have been made with other fluorescent molecules whose fluorescence intensity increases on binding to a substrate,[20,31] but since only the dye is present in aqueous solution this too is unlikely. It is possible that under laser irradiation the compound undergoes a photocatalysed transformation to a more intensely fluorescent species.[32] Although there was no change in the observed emission maximum, this should not be ruled out. Increases in fluorescence intensity have been induced using pulsed lasers by Hell and coworkers,[33] but in this case the laser irradiation was continuous. A further study is required to determine the precise cause of this phenomenon.

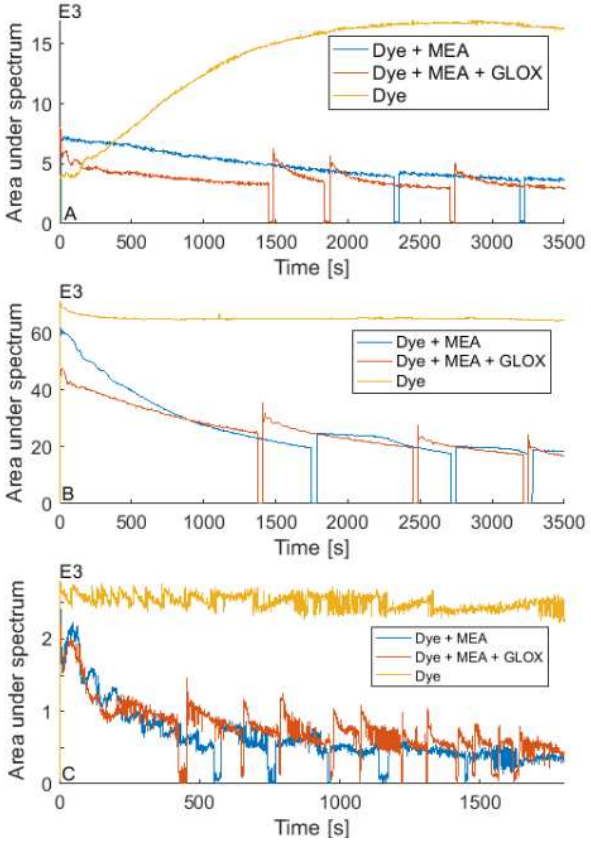

Figure 2. Bleaching and reactivation graphs for **1** (A), **2** (B), and **3** (C).

The introduction of additives (MEA and GLOX) triggered photobleaching and the average rate of recovery dramatically increased under GLOX buffered conditions (Table 3) confirming GLOX to be a superior buffer system for reversible photoblinking as required for STORM imaging.[34]

Table 3. Results of reversible bleaching experiments.

Dye [a]	Buffer [b]	Decay rate (× 10^{-3} s^{-1})	Avg. recovery (%)	Avg. PEL (%) [c]
1	A	0.265	12	-
	B	1.21	78	15
2	A	0.555	12	-

	B	0.439	48	15
	A	2.06	15	-
3				
	B	10.0	81	24

[a] All dye solutions were diluted to 1 × 10^{-5} M. Recorded using OceanView and analysed using Matlab.[35] [b] A: Dye solution with MEA (0.1 M); B: Dye solution with MEA (0.1 M) and GLOX buffer. [c] Calculated as a percentage of fluorescence intensity decay before the rate of decay slowed and became exponential.

It was noted for each dye that when using GLOX buffer there was a sharp drop in fluorescence intensity prior to exponential decay (pre-exponential loss, PEL).

After solution phase analysis was complete, the blinking activity and hence suitability for super resolution microscopy was assessed by adopting a method recently described by Gibbs, *et al*. by immobilisation of the dyes in a polyvinyl alcohol (PVA) matrix.[36] The properties analysed for each dye were the average number of blinking events per μm^2 area, the average length of continuous emission (on time), and the number of times blinking molecules switched between their 'on' and 'off' states (number of cycles, Table 4). On time and number of cycles were determined by first plotting *z*-axis profiles of pixel intensity for individual blinking molecules (Figure 3).

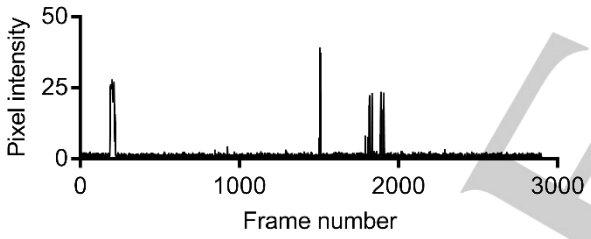

Figure 3. Representative *z*-axis profile for an individual photoblinking molecule of **1**. Frame rate = 20 Hz.

The *z*-axis profiles can in turn be simplified to so-called 'on/off trajectories' in which any signal above a specified threshold is denoted 'on' giving a binary trace. In this case, the threshold was set to detection of pixel intensity of 5, and this was used to determine the on time and number of cycles for each molecule. Representative on/off trajectories are provided for each compound (Figure 4).

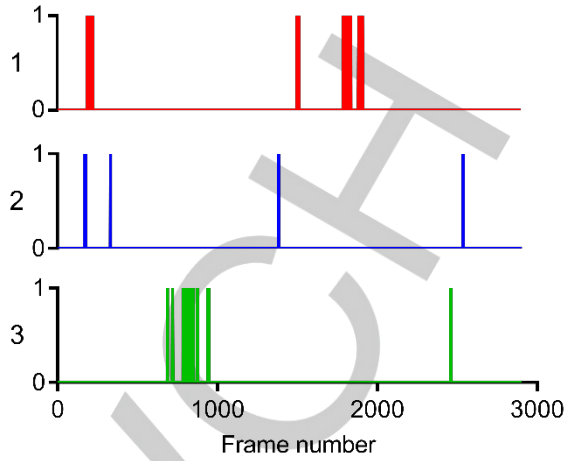

Figure 4. Representative on/off trajectories for individual photoblinking molecules of **1** (top), **2** (centre), and **3** (bottom). Frame rate = 20 Hz.

Dyes **1**–**3** displayed no trend in blink density between buffer systems. NBD-APTES **1** displayed a higher blinking density in the presence of MEA and without GLOX buffer, and this result was reversed in molecules containing heavier atoms.

Table 4. Results of blink analysis for each dye for compounds **1**, **2**, and **3**.

Dye [a]	Buffer [b]	Avg. blink density [μm^{-1}] [c]	Avg. on time [s] [d]	Avg. Number of cycles [d]
1	A	1.40	0.19	2.9
	B	1.16	0.39	4.9
2	A	1.30	0.22	1.4
	B	2.00	0.33	3.0
3	A	1.01	0.11	1.5
	B	1.46	0.34	2.9

[a] All dye solutions were diluted to 3 × 10^{-8} M. Andor Solis was used with Fiji,[37,38] and the ThunderSTORM plugin to record and analyse blinking data.[39] [b] A: Dye solution with MEA (0.1 M); B: Dye solution with MEA (0.1 M) and GLOX buffer. [c] Calculated as an average of the number of blinking events captured within a specified area over the duration of the experiment. [d] Calculated by plotting *z*-axis profiles of pixel intensity for individual molecules.

For **2**, this is believed to be because sulfur atoms enable the stabilisation of electronic 'dark' states,[40] however, although this area has not been investigated with organoselenides, it is feasible that selenium may offer the same effect. In all three cases, both the average 'on' time average number of cycles were increased in the presence of GLOX buffer. NBD-APTES **1** was vastly more active under both sets of conditions than NPT and NPSe-APTES (**2** and **3** respectively), which showed similar

results for both variables. These results correlate with the excited state lifetimes observed. The enhanced blink rate may also explain why the oxygen containing NBD moiety has not successfully been used for SMLM imaging. If the oxygen analogue **1** is used to densely label a sample (as is required for SMLM imaging), too many fluorophores in the sample blink simultaneously and localisation cannot occur. However, it may have better compatibility with other techniques such as super-resolution radial fluctuation or 3B, an SMLM software package capable of localising overlapping fluorophores.

Since the lengths of the dark states for each dye are long-lasting (several seconds) it is likely that the blinking mechanism is redox based.[41] Such reversible redox reactions of dyes with MEA *via* photoinduced electron transfer that result in non-fluorescent radical ions are more likely to occur from the triplet state.[10,41] The heavier atoms in the sulfur and selenium containing dyes stabilize the triplet state, promoting transition to the dark state, that in turn results in longer dark states and fewer observed localisation events. Further analyses were undertaken to establish the number of photons detected per blinking event and the average on/off duty cycle (fraction of time spent in the 'on' state after equilibrium is reached) over the duration of the 150 s experiment (Table 5).

Table 5. Further blink analysis for compounds **1**, **2**, and **3**.

Dye [a]	Buffer [b]	Avg. photons detected per blink [c]	Avg. on/off duty cycle
1	A	182	0.0013
	B	889	0.0027
2	A	514	0.0015
	B	875	0.0023
3	A	164	0.00078
	B	468	0.0023

[a] All dye solutions were diluted to 1 × 10^{-5} M. FITC filter cube was used. Andor Solis was used with Fiji,[37,38] and the ThunderSTORM plugin to record and analyse blinking data.[39] [b] A: Dye solution with MEA (0.1 M); B: Dye solution with MEA (0.1 M) and GLOX buffer. [c] Calculated based on the analog-to-digital ratio for the camera used (Andor Zyla sCMOS) being 0.28 as stated in the manufacturers specifications.

The average on/off duty cycles (fraction of time in the on state) for each of the dyes in this study are comparable and similar to the top performing dyes currently used for STORM, as analysed by Dempsey and coworkers.[42] The average numbers of photons observed per blinking event is lower than, but of the same magnitude, as other dyes that absorb in the blue region of the visible spectrum.[42] The dyes also perform similarly in this respect when compared to commonly used SMLM dyes suspended in PVA matrices.[36] This study has shown that sufficient photons can be detected for fluorescence to be distinguished from background noise and subsequent localisation of individual molecules. Although the quantum yields are low, this is not problematic for SMLM imaging, as many of the commonly used dyes have wide ranging quantum yields.[42] While under ideal SMLM conditions (with MEA and GLOX buffer) **1** and **2** performed similarly, **3** appeared to emit far fewer photons, and this may be due to the poor overlap of available laser wavelengths with the absorption spectrum of **3**. Molecules stochastically blinked throughout the whole duration of these experiments.

Armed with the knowledge of how individual molecules in sparsely populated samples behave, it was then prudent to see if these results could be used to predict the suitability of a dye to take images of small structures using SMLM techniques. Silica nanoparticles were synthesised *via* Stöber synthesis in which the silane functionalised dyes were added at a later stage to coat the surface (Scheme 3).

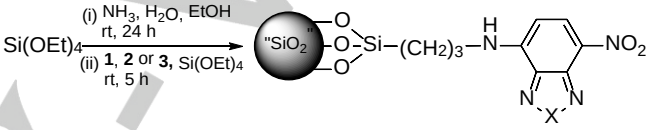

Scheme 3. Synthesis of fluorescent nanoparticles. X = O (**1**), S (**2**), or Se (**3**).

As well as the nanoparticles being visibly coloured after functionalisation, coating was confirmed using fluorimetry. The average size and spherical shape of the particles were confirmed using dynamic light scattering (see supplementary information) and scanning electron microscopy (Figure 5). The average diameter of nanoparticles coated with **1**, **2** and **3** were 239.8, 223.3 and 256.4 nm, respectively.

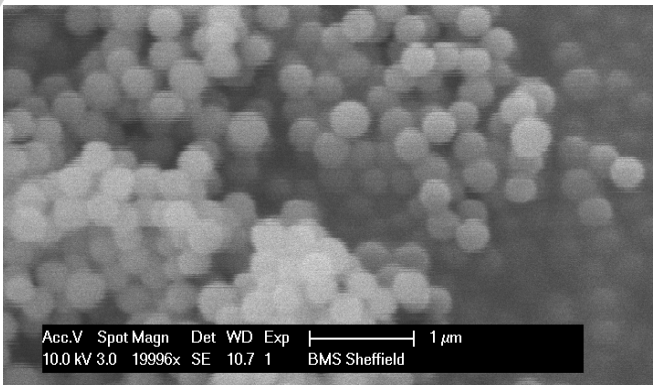

Figure 5. Scanning electron micrograph of silica nanoparticles coated with **1**. Scale bar 1 µm.

When viewed under an epifluorescence microscope, the stochastic photoswitching process easily allowed for loose molecules to be localised and ignored as noise whereas when a

large number of fluorophores were present on a nanoparticle it was possible to detect them as separate entities (Figure 6).

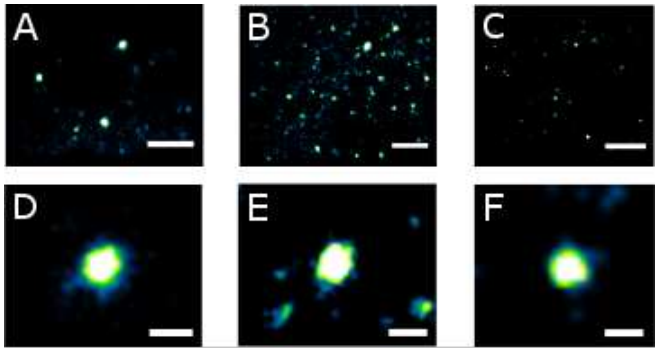

Figure 6. Reconstructed wide field (1.0 µm scale, A – C) and close up images of silica nanoparticles (0.2 µm scale, D – F) coated with NBD-APTES **1** (A, D), NPT-APTES **2** (B, E), and NPSe-APTES **3** (C, F).

As observed in the solution phase bleaching experiments, nanoparticle bound NBD-APTES **1** stopped photoswitching and showed a dramatic increase in fluorescence intensity with continued laser irradiation throughout data acquisition, even at low laser power. Similarly to the solution phase experiments, this was not observed with nanoparticle bound NPT-APTES **2** or NPSe-APTES **3**.

Conclusions

In summary, modification of the aromatic systems by the introduction of larger atoms in this series of dye molecules gave rise to minor perturbations in the internal angle of the five-membered ring (however, the molecules do remain planar) which, when combined with an increased degree of aromaticity, resulted in significant changes in their photophysical properties. Integral properties such as extinction coefficient, quantum yield and excited state lifetime were all reduced in dyes containing heavier atoms. These properties correlated with the observed photoblinking behaviour. Blinking density in the two buffers tested was lower in GLOX buffer for NBD-APTES **1** but higher for NPT- and NPSE-APTES (**2** and **3**) since the heavy atom stabilisation afforded by the presence of sulfur and selenium meant that those dye molecules were less likely to blink unless in an environment which encourages them to do so. The oxygen containing dye has the most stable excited state lifetime, meaning it is more likely to fluoresce than exist in its dark state, unless in the presence of GLOX buffer.

As for the suitability of each dye for super-resolution microscopy, the faster blink rate of the oxygen containing NBD-APTES **1** is actually its downfall. Although in this study it was possible to analyse the blinking of each dye since the molecules were very sparsely distributed, in reality when attempting to image densely labelled specimens (as is required for SMLM) too many dye molecules exist in the 'on' state at any given time and as such individual molecules cannot be localised. This, combined with the increase in fluorescence intensity with prolonged laser exposure, makes derivatives of **1** unsuitable as a dye for capturing SMLM images. The slower blink rate of NPT- and NPSe-APTES (**2** and **3**) make them more suited for super-resolution microscopy, however due to the relative ease in synthetic manipulation of the sulfur containing dye **2**, and given its performance compared to existing dyes used for SMLM, the organosulfur compound is much more amenable for widespread use as an SMLM dye.

Experimental Section

All starting materials were purchased from Sigma-Aldrich, Alfa Aesar or Fluorochem and used as purchased. Air sensitive reactions were conducted in flame-dried glassware under an inert atmosphere of an inert gas. 1H and 13C NMR spectra were recorded in CDCl3, MeOD, or [D_6]DMSO as specified on a Bruker 400 MHz spectrometer. Chemical shifts are recorded on the δ scale relative to the residual solvent peak and coupling constant (*J*) values are reported in Hz. Liquid chromatographic mass spectrometry (LCMS) was performed via electron ionisation (EI), electrospray ionisation (ES), affinity purification (AP) or direct infusion using either a Walter ITC Premier XE instrument or a Micromass LCT instrument. Infrared spectra were obtained using a Perkin-Elmer RX1 FT-IR spectrometer with a Sinsir Technologies DuraSimlir II ATR attachment. UV/vis absorption spectra were measured using a Cary Bio 3 spectrophotometer. Excitation and emission spectra were recorded a Fluoromax Fluorometer. Dynamic light scattering data was collected using a Malvern Zetasizer NanoZS instrument. Confocal microscopy images were taken using a wide-field Delta Vision confocal microscope. Scanning electron microscopy images were taken using a Philips XL-20 SEM. Melting points were measured using a Gallenkamp melting point apparatus. Dye photobleaching data was recorded using Ocean Optics STS-VIS Miniature Spectrometer. Blink rate analysis was undertaken using a Nikon Eclipse Ti microscope coupled to a Andor Zyla sCMOS camera.

Geometry optimisations were calculated using Gaussian 09 using density functional theory (DFT) with a B3LYP 6311g (d,p) basis set. Energy levels were calculated using a time-dependant self-contained field (TD-SCF) DFT with a B3LYP 6311g (d,p) basis set and was solved for N = 100 states.

Data for time-resolved photoluminescence lifetimes was obtained using the time-correlated single photon counting (TCSPC) method. The samples were excited with a pulsed laser of 510 nm, repetition rate 2.5 MHz, average power <4 mW, pulse width <60 ns. The PL was detected with a single photon avalanche diode, which has an instrument response function that was measured to be around 1 ns.

7-Nitro-*N*-[3-(triethoxysilyl)propyl]-2,1,3-benzoxadiazol-4-amine (1): A sample of 4-chloro-7-nitrobenzo-2,1,3-oxadiazole (0.10 g, 0.5 mmol) was stirred in ethanol (10 mL). Once dissolved, the solution was cooled to 0 ℃ and 3-aminopropyltriethoxysilane (0.14 mL, 0.6 mmol, 1.2 eq) was added. The reaction mixture was stirred in the dark for 2 h at 0 ℃ then for 24 h at room temperature during which time the mixture turned from yellow to dark green. The solvent was removed *in vacuo* to leave a dark green residue which was purified by column chromatography on silica, eluting with petroleum ether/ethyl acetate 2:1 to yield the product as an orange/red solid (0.10 g, 48%); m.p. 110–114 ℃; R_f = 0.73 (petroleum ether: ethyl acetate 2:1); ^{1}H NMR (400 MHz, $CDCl_3$): 8.48 (1H, d, *J* 8.7, ArC*H*), 6.95 (1H, s, N*H*), 6.17 (1H, d, *J* 8.7, ArC*H*), 3.86 (6H, q,

J 7.0, 3 × OC*H*$_2$CH$_3$), 3.61–3.50 (2H, m, NHC*H*$_2$), 2.04–1.93 (2H, m, C*H*$_2$), 1.24 (9H, t, *J* 7.0, 3 × OCH$_2$C*H*$_3$), 0.77 (2H, t, *J* 7.6, SiC*H*$_2$); *m/z* (ES$^+$) 439 (8%), 407 (100, M+Na$^+$), 393 (8), 339 (22, M$^+$-OEt), 235 (5), 210 (5); HRMS: found 407.1379, M+Na$^+$. $C_{15}H_{24}N_4O_6NaSi$ requires 407.1363). Data was in accordance with the literature.[23]

4-Bromo-7-nitro-2,1,3-benzothiadiazole (4): 4,7-Dibromobenzo-2,1,3-thiadiazole (0.10 g, 0.34 mmol) was dissolved in nitric acid (68%, 5 mL). The mixture was stirred at reflux for 2 h during which time the solution changed colour from orange to pale yellow. The hot solution was poured onto ice-water (10 mL) and produced a pale yellow precipitate. Filtration and drying afforded the product as a pale yellow crystalline solid which was used without further purification (0.03 g, 40%); m.p. 218–220 ℃ (lit.[43] 218–220 °C); ^{1}H NMR (400 MHz, CDCl$_3$): 8.47 (1H, d, *J* 8.0, ArC*H*), 8.03 (1H, d, *J* 8.0, ArC*H*); ^{13}C NMR (100 MHz, [D$_6$]DMSO): 154.4 (Ar*C*), 145.8 (Ar*C*), 139.1 (Ar*C*), 131.4 (Ar*C*H), 128.8 (Ar*C*H), 122.3 (Ar*C*); *m/z* (EI$^+$) 261 (48%, $C_6H_2N_3O_2S^{81}Br$), 259 (47), 231 (81), 229 (80), 203 (46), 201 (43), 134 (100), 83 (88). Data in accordance with the literature.[44]

7-Nitro-*N*-[3-(triethoxysilyl)propyl]-2,1,3-benzothiadiazole-4-amine (2): A sample of bromide **4** (0.030 g, 0.12 mmol) was dissolved in ethanol (10 mL) with (3-aminopropyl)triethoxysilane (0.034 g, 0.15 mmol, 1.25 eq) and cooled with stirring to 0 ℃ in the dark. Solid potassium carbonate (0.017 g, 0.012 mmol, 0.1 eq) was added to the stirred solution which was kept at 0 ℃ for 2 h before allowing the reaction to proceed at room temperature for a further 22 h, during which time the reaction mixture turned from yellow to green. The solvent was removed under reduced pressure and the residue re-dissolved in ethyl acetate (25 mL). This solution was washed with water (2 × 25 mL) and brine (2 × 25 mL), dried over MgSO$_4$, filtered and concentrated *in vacuo*, followed by purification using column chromatography on silica gel to give the title compound as a dark orange solid; (0.022 g, 45%); m.p. 100–102 ℃; R$_f$ = 0.51 (petroleum ether: ethyl acetate 3:1); ν_{max} (ATR)/cm^{-1} 3339 (br, NH), 2972 (w, CH), 2885 (w, CH), 1563 (s, NO$_2$), 1493 (s); ^{1}H NMR (400 MHz, CDCl$_3$): 8.67 (1H, d, *J* 8.8, ArC*H*), 6.65 (1H, br t, *J* 5.1, N*H*), 6.41 (1H, d, *J* 8.8, ArC*H*), 3.86 (6H, q, *J* 7.0, 3 × OC*H*$_2$CH$_3$), 3.53 (2H, q, *J* 7.1, NHC*H*$_2$), 1.95 (2H, pent, *J* 7.1, C*H*$_2$), 1.24 (9H, t, *J* 7.0, 3 × OCH$_2$C*H*$_3$), 0.81–0.77 (2H, m, SiC*H*$_2$); ^{13}C NMR (100 MHz, CDCl$_3$): 148.3 (Ar*C*), 146.7 (Ar*C*), 146.5 (Ar*C*), 134.0 (Ar*C*H), 128.3 (Ar*C*), 98.9 (Ar*C*H), 58.6 (3 × O*C*H$_2$), 45.6 (*C*H$_2$), 22.2 (*C*H$_2$), 18.3 (3 × *C*H$_3$), 7.8 (*C*H$_2$); *m/z* (ESI$^+$) 446 (6), 401.1313 (100%, MH$^+$ $C_{15}H_{25}N_4O_5SSi$ requires 401.1309), 355 (16).

3-Bromo-6-nitro-1,2-benzenediamine (5): 1-Amino-2-bromo-5-nitrobenzene (0.25 g, 1.15 mmol) was dissolved in dry dimethyl sulfoxide (15 mL) at room temperature under an atmosphere of argon. 1,1,1-Trimethylhydrazinium iodide (0.23 g, 1.15 mol, 1 eq) was added in one portion before adding fresh sodium pentoxide (0.38 g, 3.45 mmol, 3 eq). The solution turned from orange to dark blue on immediate addition of the base. The reaction was stirred overnight at room temperature before pouring onto ice water (50 mL). The product was extracted with dichloromethane (2 × 25 mL) and the organic layers washed with hydrochloric acid (1M, 2 × 25 mL) and brine (25 mL) before drying over magnesium sulfate, filtering and removing solvent *in vacuo* to give the product as a dark orange solid which was used without further purification (0.078 g, 30%); m.p. 145–148 °C; ν_{max} (ATR)/cm^{-1} 3465 (w, NH), 3422 (w, NH), 3358 m, NH), 1620 (s, NH), 1556 (m), 1505 (s, NO$_2$); ^{1}H NMR (400 MHz, CDCl$_3$): 7.62 (1H, d, *J* 9.3, ArC*H*), 6.91 (1H, d, *J* 9.3, ArC*H*), 6.16 (2H, br s, N*H*$_2$), 3.95 (2H, br s, N*H*$_2$); ^{13}C NMR (100 MHz, [D$_6$]DMSO): 135.9 (Ar*C*), 135.2 (Ar*C*), 130.4 (Ar*C*), 119.3 (Ar*C*H), 113.9 (Ar*C*H), 111.9 (Ar*C*); *m/z* (ESI$^+$) 233.9698 (95%, MH$^+$, $C_6H_7N_3O_2^{81}Br$ requires 233.9696), 232 (100, $C_6H_7N_3O_2^{79}Br$). ^{1}H NMR data was not in accordance with that in the literature, and so full analysis was undertaken.[24]

4-Bromo-7-nitro-2,1,3-selenadiazole (6): Diamine **5** (0.16 g, 0.71 mmol) was dissolved in ethanol (40 mL) and heated at reflux. A solution of selenium dioxide (0.39 g, 3.55 mmol, 5 eq) in boiling water (20 mL) was added over 5 mins to the reaction mixture and on complete addition a yellow precipitate began to form. The mixture was maintained at reflux for a further 16 h before cooling to rt. The precipitate was isolated *via* vacuum filtration and washed with ice-cold water (2 × 10 mL) to give the title product as a mustard yellow solid which was used without further purification (0.19 g, 85%); m.p. 282–284 ℃ (decomp.), lit. [45] >300 °C; Found: C, 23.4; H, 0.95; N, 13.55; Br, 26.1. $C_6H_2N_3O_2SeBr$ requires C, 23.5; H, 0.7; N, 13.7; Br, 26.0%; ν_{max} (ATR)/cm^{-1} 3461 (w), 3422 (w), 3357 (m), 3255 (w), 1618 (s), 1506 (s, NO$_2$); ^{1}H NMR (400 MHz, [D$_6$]DMSO): 8.39 (1H, d, *J* 8.0, ArC*H*), 8.12 (1H, d, *J* 8.0, ArC*H*); ^{13}C NMR (100 MHz, [D$_6$]DMSO): 157.7 (Ar*C*), 149.3 (Ar*C*), 140.3 (Ar*C*), 129.5 (Ar*C*H), 127.4 (Ar*C*H), 123.8 (Ar*C*); *m/z* (EI$^+$) 306.8486 (76%, M$^+$ $C_6H_2N_3O_2^{80}Se^{79}Br$ requires 306.8490), 277 (100), 248 (50), 182 (62), 159 (29), 131 (19), 101 (33), 80 (34). ^{1}H NMR and IR spectra in broad agreement with the literature – not other data is reported.[45]

7-Nitro-*N*-[3-(triethoxysilyl)propyl]-2,1,3-benzoselenadiazol-4-amine (3): *tris*-(Dibenzylideneacetone)dipalladium (0.0046 g, 0.005 mmol, 2 mol%) and (*S*)-(+)-PPFA (0.0062 g, 0.014 mmol, 6 mol%) were dissolved in dry THF (1 mL) in a microwave vial. Bromide **6** (0.070 g, 0.228 mmol) and APTES (0.061 g, 0.274 mmol, 1.2 eq) were added to the solution before charging the solution with potassium *tert*-butoxide (0.033 g, 0.342 mmol, 1.5 eq). The solution was degassed with argon for 15 mins. The tube was sealed and heated in a microwave reactor to 75 °C over 5 mins at 150 W, then held at this temperature for a further 9 mins at 100 W. On completion, the reaction mixture was diluted with ethyl acetate (10 mL) and filtered. The filtrate was evaporated to dryness before purifying the crude product on silica gel (1:1 petroleum ether/ethyl acetate) to give the product as a red/orange solid. (0.0015 g, 7%); R$_f$ = 0.56 (petroleum ether/ethyl acetate); m.p. 68–71^{o}C; ν_{max} (ATR)/cm^{-1} 3465 (w, NH), 3361 (m, NH), 2926 (m), 1621 (s, C=N), 1511 (s, NO$_2$); ^{1}H NMR (500 MHz, CDCl$_3$): 8.62 (1H, d, *J* 8.8, ArC*H*), 6.65–6.61 (1H, m, N*H*), 6.17 (1H, d, *J* 8.8, ArC*H*), 3.78 (6H, q, *J* 7.4, 3 × C*H*$_2$CH$_3$), 3.42 (2H, q, *J* 6.4, NC*H*$_2$), 1.85 (2H, q, *J* 7.5, C*H*$_2$), 1.18 (9H, t, *J* 7.0, 3 × C*H*$_3$), 0.71–0.68 (2H, m, SiC*H*$_2$); ^{13}C NMR (125 MHz, CDCl$_3$): 152.7 (Ar*C*), 152.5 (Ar*C*), 147.5 (Ar*C*), 135.7 (Ar*C*H), 129.9 (Ar*C*), 97.2 (Ar*C*H), 58.6 (3 × O*C*H$_2$), 45.7 (NC*H*$_2$), 22.3 (*C*H$_2$), 18.3 (3 × *C*H$_3$), 7.9 (Si*C*H$_2$); *m/z* (ESI$^+$) 449.0757 (100%, MH$^+$, $C_{15}H_{25}N_4O_5Si^{80}Se$ requires 449.0754).

General procedure for the preparation of dye coated silica nanoparticles: Tetraethyl orthosilicate (TEOS, 1.7 mL, 7.6 mmol) was added to a stirred mixture of water (4.5 mL) and ammonium hydroxide (35%, 330 μL) in ethanol (43.5 mL). The mixture was stirred rapidly at room temperature for 24 h, after which a solution of APTES conjugated dye in ethanol (18 mM, 50 μL) was added with additional TEOS (10 μL). The particles were left to stir with the dye for 5 h at rt. Coated particles were isolated by centrifugation, re-suspended in ethanol (30 mL), isolated by centrifugation, re-suspended again in water (30 mL), and isolated by centrifugation.

Preparation of buffers for photophysical analysis: Aqueous stock solutions of catalase from bovine liver (4 mg per 1 mL), glucose oxidase from *Aspergillus niger* (5 mg per 1 mL) and mercaptoethylamine (MEA, 1 M) were prepared.

To make 10 mL MEA buffer: take 1 mL MEA stock and make up to 10 mL with distilled water.

To make 10 mL GLOX buffer: take 1 mL MEA stock, 1 mL glucose oxidase stock, 0.1 mL catalase stock and make up to 10 mL with distilled water. Add solid glucose (1 g, 10% w/v).

General procedure for the preparation and imaging of PVA suspensions: Fluorophores were diluted to a nanomolar concentration in 1 wt% PVA (48,000 MW) in distilled water. 50 µL was added to each slide before air-drying in a fume hood overnight. Samples were imaged between 30 and 60 mins after buffer solution (MEA or GLOX, 15 µL) was added to allow sufficient time for matrix penetration but to avoid rehydration and degradation of the polymer. Slides sealed with a cover slip and 740 clear Rimmel London 60 second nail polish.

Each sample was imaged twice in two different regions of the matrix under each buffer condition. Two samples were imaged for each dye/buffer combination. Samples were excited using a 470 nm laser with a power of 550 mW. Imaging videos were captured at a rate of 20 frames per second for 3000 frames. The ThunderSTORM plugin for Fiji was used to analyse captured data.

Acknowledgements

The authors would like to thank Dr. Anthony Meijer for his guidance in geometry optimisation and energy calculations. Dr. D. M. Coles and Claire Greenland measured quantum yields and excited state lifetimes, respectively. DRJ is funded by the EPSRC at the Molecular Scale Engineering Centre for Doctoral Training (EP/J500124/1).

Keywords: Dyes/Pigments • Nanoparticles • Atomic Substitution • Super-Resolution Microscopy • Photoblinking

[1] H. Popper, *Physiol. Rev.* **1944**, *24*, 205–224.
[2] S. Strugger, *Can. J. Res.* **1948**, *26*, 188–193.
[3] P. Ellinger, *Biol. Rev.* **1940**, *15*, 323–347.
[4] E. Abbe, *Arch. für Mikroskopische Anat.* **1873**, *9*, 413–418.
[5] M. J. Rust, M. Bates, X. Zhuang, *Nat. Methods* **2006**, *3*, 793–796.
[6] E. Betzig, G. H. Patterson, R. Sougrat, O. W. Lindwasser, S. Olenych, J. S. Bonifacino, M. W. Davidson, J. Lippincott-Schwartz, H. F. Hess, *Science* **2006**, *313*, 1642–1645.
[7] S. T. Hess, T. P. K. Girirajan, M. D. Mason, *Biophys. J.* **2006**, *91*, 4258–4272.
[8] D. N. Dempster, T. Morrow, R. Rankin, G. F. Thompson, *J. Chem. Soc. Faraday Trans. 2 Mol. Chem. Phys.* **1972**, *68*, 1479–1496.
[9] M. Bates, T. Blosser, X. Zhuang, *Phys. Rev. Lett.* **2005**, *94*, 108101.
[10] R. Zondervan, F. Kulzer, S. B. Orlinskii, M. Orrit, *J. Phys. Chem. A* **2003**, *107*, 6770–6776.
[11] M. S. Afzal, J.-P. Pitteloud, D. Buccella, *Chem. Commun. (Camb).* **2014**, *50*, 11358–61.
[12] N. R. Conley, A. Dragulescu-Andrasi, J. Rao, W. E. Moerner, *Angew. Chemie - Int. Ed.* **2012**, *51*, 3350–3353.
[13] M. R. Detty, P. N. Prasad, D. J. Donnelly, T. Ohulchanskyy, S. L. Gibson, R. Hilf, *Bioorganic Med. Chem.* **2004**, *12*, 2537–2544.
[14] Y. S. Park, T. S. Kale, C.-Y. Nam, D. Choi, R. B. Grubbs, *Chem. Commun. (Camb).* **2014**, 7964–7967.
[15] A.-M. Kelterer, A. Mansha, F. J. Iftikhar, Y. Zhang, W. Wang, J.-H. Xu, G. Grampp, *J. Mol. Model.* **2014**, *20*, 2344.
[16] A. T. Balaban, D. C. Oniciu, A. R. Katritzky, *Chem. Rev.* **2004**, *104*, 2777–2812.
[17] A. R. Katritzky, I. P. Barczynski, G. Musumarra, D. Pisano, M. Szafranll, *J. Am. Chem. Soc.* **1989**, *111*, 7–15.
[18] A. R. Katritzky, P. Barczynski, *J. Prakt. Chem.* **1990**, *332*, 885–897.
[19] C. W. Bird, *Tetrahedron* **1992**, *48*, 335–340.
[20] Y. Shen, Y. Zhang, X. Zhang, C. Zhang, L. Zhang, J. Jin, H. Li, S. Yao, *Anal. Methods* **2014**, *6*, 4797–4802.
[21] Y. Koide, Y. Urano, K. Hanaoka, T. Terai, T. Nagano, *ACS Chem. Biol.* **2011**, *6*, 600–8.
[22] M. J. Frisch, G. W. Trucks, H. B. Schlegel, G. E. Scuseria, M. A. Robb, J. R. Cheeseman, G. Scalmani, V. Barone, B. Mennucci, G. A. Petersson, et al., *Gaussian, Inc.* **2009**.
[23] B. Liu, F. Zeng, G. Wu, S. Wu, *Chem. Commun. (Camb).* **2011**, *47*, 8913–5.
[24] U. Baettig, I. Bruce, N. J. Press, S. J. Watson, *PCT Int. Appl.* **2010**, WO2010063802A1.
[25] T. Wang, D. R. Magnin, L. G. Hamann, *Org. Lett.* **2003**, *5*, 897–900.
[26] J. Jona, W. Derbyshire, H. S. Gutowsky, *J. Phys. Chem.* **1965**, *69*, 1.
[27] Y. Yamashita, K. Ono, M. Tomura, S. Tanaka, *Tetrahedron* **1997**, *53*, 10169–10178.
[28] N. Nijegorodov, R. Mabbs, *Spectrochim. Acta - Part A Mol. Biomol. Spectrosc.* **2001**, *57*, 1449–1462.
[29] T. Y. Ohulchanskyy, D. J. Donnelly, M. R. Detty, P. N. Prasad, *J. Phys. Chem. B* **2004**, *108*, 8668–8672.
[30] M. Heilemann, S. van de Linde, A. Mukherjee, M. Sauer, *Angew. Chem. Int. Ed. Engl.* **2009**, *48*, 6903–8.
[31] S. Stimpson, D. R. Jenkinson, A. Sadler, M. Latham, D. A. Wragg, A. J. H. M. Meijer, J. A. Thomas, *Angew. Chemie Int. Ed.* **2015**, *54*, 3000–3003.
[32] E. Laureto, M. A. T. Da Silva, R. V. Fernandes, J. L. Duarte, I. F. L. Dias, H. De Santana, A. Marletta, *Synth. Met.* **2011**, *161*, 87–91.
[33] G. Donnert, C. Eggeling, S. W. Hell, *Nat. Methods* **2007**, *4*, 81–86.
[34] M. Heilemann, E. Margeat, R. Kasper, M. Sauer, P. Tinnefeld, *J. Am. Chem. Soc.* **2005**, *127*, 3801–3806.
[35] *MathWorks Inc.* **2016**.
[36] A. M. Bittel, A. Nickerson, I. S. Saldivar, N. J. Dolman, X. Nan, S. L. Gibbs, *Sci. Rep.* **2016**, *6*, 29687.
[37] C. A. Schneider, W. S. Rasband, K. W. Eliceiri, *Nat. Methods* **2012**, *9*, 671–675.
[38] J. Schindelin, I. Arganda-Carreras, E. Frise, V. Kaynig, M. Longair, T. Pietzsch, S. Preibisch, C. Rueden, S. Saalfeld, B. Schmid, et al., *Nat. Methods* **2012**, *9*, 676–682.
[39] M. Ovesný, P. Křížek, J. Borkovec, Z. Švindrych, G. M. Hagen, *Bioinformatics* **2014**, *30*, 2389–2390.
[40] S. Mai, M. Pollum, L. Martínez-Fernández, N. Dunn, P. Marquetand, I. Corral, C. E. Crespo-Hernández, L. González, *Nat. Commun.* **2016**, *7*, 13077.
[41] T. Ha, P. Tinnefeld, *Annu. Rev. Phys. Chem.* **2012**, *63*, 595–617.
[42] G. T. Dempsey, J. C. Vaughan, K. H. Chen, M. Bates, X. Zhuang, *Nat. Methods* **2011**, *8*, 1027–36.
[43] V. G. Pesin, A. M. Khaletskii, V. A. Sergeev, *Zhurnal Obs. Khimii* **1963**, *33*, 1759–1766.
[44] M. Pagano, D. Castagnolo, M. Bernardini, A. L. Fallacara, I. Laurenzana, D. Deodato, U. Kessler, B. Pilger, L. Stergiou, S. Strunze, et al., *ChemMedChem* **2014**, *9*, 129–150.
[45] R. Edwards, I. Cummins, P. Steel, *PCT Int. Appl.* **2009**, WO2009034396A2.

10.1002/chem.201702289

WILEY-VCH

Entry for the Table of Contents (Please choose one layout)

Layout 1:

FULL PAPER

4-Nitrobenzodiazoles with atomic substitution through the chalcogen group were synthesised and analysed for use in single-molecule localisation microscopy. Reversible photoswitching was achieved and images of silica nanoparticles coated with each dye were captured. Dyes containing larger atoms were favoured, but the sulfur derivative was preferred due to synthetic ease.

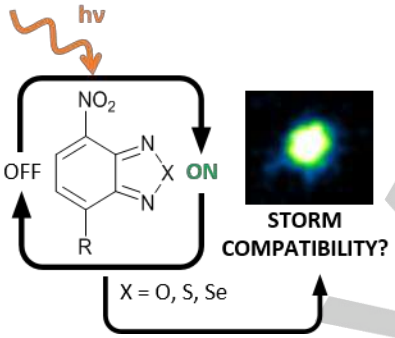

D. R. Jenkinson, A. J. Cadby, and S. Jones**

Page No. – Page No.

The synthesis and photophysical analysis of a series of 4-nitrobenzochalcogenadiazoles for super-resolution microscopy